ADVANCED FUNCTIONAL MATERIALS
www.afm-journal.de

Structural Aspects of P2-Type $Na_{0.67}Mn_{0.6}Ni_{0.2}Li_{0.2}O_2$ (MNL) Stabilization by Lithium Defects as a Cathode Material for Sodium-Ion Batteries

Liangtao Yang, Liang-Yin Kuo, Juan Miguel López del Amo, Prasant Kumar Nayak, Katherine A. Mazzio, Sebastian Maletti, Daria Mikhailova, Lars Giebeler, Payam Kaghazchi, Teófilo Rojo, and Philipp Adelhelm**

A known strategy for improving the properties of layered oxide electrodes in sodium-ion batteries is the partial substitution of transition metals by Li. Herein, the role of Li as a defect and its impact on sodium storage in P2-$Na_{0.67}Mn_{0.6}Ni_{0.2}Li_{0.2}O_2$ is discussed. In tandem with electrochemical studies, the electronic and atomic structure are studied using solid-state NMR, operando XRD, and density functional theory (DFT). For the as-synthesized material, Li is located in comparable amounts within the sodium and the transition metal oxide (TMO) layers. Desodiation leads to a redistribution of Li ions within the crystal lattice. During charging, Li ions from the Na layer first migrate to the TMO layer before reversing their course at low Na contents. There is little change in the lattice parameters during charging/discharging, indicating stabilization of the P2 structure. This leads to a solid-solution type storage mechanism (sloping voltage profile) and hence excellent cycle life with a capacity of 110 mAh g^{-1} after 100 cycles. In contrast, the Li-free compositions $Na_{0.67}Mn_{0.6}Ni_{0.4}O_2$ and $Na_{0.67}Mn_{0.8}Ni_{0.2}O_2$ show phase transitions and a stair-case voltage profile. The capacity is found to originate from mainly Ni^{3+}/Ni^{4+} and $O^{2-}/O^{2-\delta}$ redox processes by DFT, although a small contribution from Mn^{4+}/Mn^{5+} to the capacity cannot be excluded.

1. Introduction

Sodium-ion batteries (SIBs) are among the most promising options for expanding the number of high performance rechargeable batteries.[1–3] While lithium-ion batteries (LIBs) provide the highest energy density, the major motivation for implementing SIB technology is the hope for lowering costs and supply risks as well as improving environmental friendliness by using more abundant elements such as Na, Mn, or Fe for the positive electrode (cathode during cell discharge).[4,5] Positive electrode materials can be classified according to their structure into four major types, i.e., polyanionic compounds, conversion materials, layered oxides, and sodium rich materials.[5,6] Among them, layered oxides are the most promising candidates, because they meet a number of application relevant parameters, such as high redox potential (vs Na^+/Na), high energy density,

Dr. L. Yang, Dr. K. A. Mazzio, Prof. P. Adelhelm
Institute of Chemistry
Humboldt-University Berlin
Brook-Taylor-Str. 2, 12489 Berlin, Germany
E-mail: philipp.adelhelm@hu-berlin.de
Dr. L. Yang
Shenzhen Institutes of Advanced Technology
Chinese Academy of Sciences
Shenzhen 518055, China
Dr. L.-Y. Kuo
Physikalische und Theoretische Chemie
Freie Universität Berlin
Arnimallee 22, 14195 Berlin, Germany

The ORCID identification number(s) for the author(s) of this article can be found under https://doi.org/10.1002/adfm.202102939.

DOI: 10.1002/adfm.202102939

Dr. L.-Y. Kuo, Dr. P. Kaghazchi
Forschungszentrum Jülich GmbH
Institute of Energy and Climate Research
Materials Synthesis and Processing (IEK-1)
52425 Jülich, Germany
E-mail: p.kaghazchi@fz-juelich.de
Dr. J. M. López del Amo, Prof. T. Rojo
Centro de Investigación Cooperativa de Energías Alternativas
(CIC energiGUNE)
Basque Research and Technology Alliance (BRTA)
Parque Tecnológico de Alava
Albert Einstein 48, Vitoria-Gasteiz 01510, Spain
Dr. P. K. Nayak
SRM Institute of Science and Technology
Kattankulathur
Chennai, Tamil Nadu 603203, India
Dr. K. A. Mazzio, Prof. P. Adelhelm
Joint reserach group Operando Battery Analysis
Helmholtz-Zentrum Berlin
Albert-Einstein-Straße 15, 12489 Berlin, Germany
S. Maletti, Dr. D. Mikhailova, Dr. L. Giebeler
Leibniz Institute for Solid State and Materials Research (IFW) Dresden e.V.
Helmholtzstraße 20, 01069 Dresden, Germany

and good cycling stability.[3,7,8] Sodium layered oxides are classified as P-type and O-type depending on the prismatic or octahedral coordination of Na^+. The most frequent ones are P2 and O3, where the numbers indicate the number of TMO layers per unit cell.[9] Structural properties of layered oxides for LIBs and SIBs have been recently discussed by Delmas et al.[10]

In view of its elemental abundance, price, and environmental friendliness, Mn-rich layered oxides are highly desirable for SIBs.[11–14] Na_xMnO_2 ($0.44 < x < 1.0$) has been intensively studied since the 1970s with varying parameters of calcination temperature, Na content, and cut-off potential.[15] Although the reported capacity values largely depend on the Na content and experimental conditions, capacity fading has been reported in all cases.[8,16,17] To mitigate this, studies on layered oxides with two $Na_xMnTM'O_2$ and three $Na_xMnTM'TM''O_2$ transition metals have been conducted and revealed that substitution (or "doping") is so far the most effective strategy to tackle the capacity fading upon cycling.[2,7a,8,14,18] Despite the well-known substitution elements such as Ni or Co, TM substitution by Li has been reported to enhance the ion storage properties.[13,19–23] An early publication on Li-substituted $Na_xLi_yNi_{0.25}Mn_{0.75}O_{2+\delta}$ by Johnson and coworkers showed a capacity of 133 mAh g^{-1}, but more than 20% of the capacity was lost after 50 cycles.[19] Studies on Li-substituted P2 and O3 cathode materials were reported by Meng and coworkers.[20,21,24] For the P2 material, Li acted as a structural stabilizer by minimizing the number of phase transformations during Na storage/release up to 4.4 V, thereby increasing the average voltage and storage capacity. The preferred location of Li^+ in this material was in the TMO layer. Similar stabilization effects were also found in Li-substituted O3 materials.[21] Minimizing the number of phase transitions during charging/discharging is generally desired for achieving a better cycle life. However, the role of lithium in the stabilization process is still unclear during de-/sodiation, and a more detailed understanding on the beneficial effects of Li as a substitutional element are worthwhile.

Herein, we unravel the beneficial role of lithium for the compound $Na_{0.67}Mn_{0.6}Ni_{0.2}Li_{0.2}O_2$ (MNL) that was synthesized using a previously reported sol-gel method followed by high temperature calcination.[5] In order to study the impact of Li-substitution at Mn or Ni sites on the structure and electrochemistry, materials with compositions of $Na_{0.67}Mn_{0.6}Ni_{0.4}O_2$ (MN32) and $Na_{0.67}Mn_{0.8}Ni_{0.2}O_2$ (MN41) were also prepared, i.e., the compound contains either additional Mn or Ni instead of Li. X-ray diffraction (XRD), scanning electron microscopy (SEM) and solid-state nuclear magnetic resonance spectroscopy (ssNMR) were used to study the structure and the morphology of the compounds as well as the lattice occupation of these two alkali ions during cycling. All as-synthesized materials have the same P2 structure, which is in line with the cationic potential concept published by Hu and coworkers (Φ_{cation} = 13.01 (MN32), 17.74 (MN41), 14.37 (MNL)).[25] In MNL, around 46% of the Li^+ occupies the Na layer and the rest is located in the TMO layer. After desodiation, the P2 phase is maintained (as confirmed by operando XRD and DFT calculations) as well as the distribution of the lithium ions (even after 10 cycles). DFT calculations suggest that the redox activity is dominated by Ni^{3+}/Ni^{4+} and $O^{2-}/O^{2-\delta}$ redox processes. However, also the Mn^{4+}/Mn^{5+} redox couple might be active in this material. MNL displays a smooth charge and discharge voltage profile with a reversible capacity of around 110 mAh g^{-1} (MNL) at 0.1 C (1 C = 100 mA g^{-1}) between 2.0-4.6 V versus Na^+/Na. Notably, the capacity retention is significantly improved to around 100% (compared to MN32 and MN46). Li_{TM} disorders the distribution of octahedral ions and Li_{Na} disorders the Na/vacancy ordering. The phase transition (P2 → O2) is mitigated, which leads to a solid-solution type mechanism for ion storage and hence improves cycle life.

2. Results and Discussion

2.1. Structural Properties of the Pristine Materials

The material was synthesized from sodium nitrate, lithium nitrate, nickel nitrate hexahydrate, and manganese acetate tetrahydrate using a sol-gel method followed by calcination at 950 °C, as described in detail in the Supporting Information. The stoichiometry of $Na_{0.67}Mn_{0.6}Ni_{0.2}Li_{0.2}O_2$ (MNL) was confirmed using ICP analysis ($Na_{0.67}Mn_{0.59}Ni_{0.20}Li_{0.20}O_2$), and the structural properties were determined using ssNMR. The ^{23}Na NMR spectrum for MNL shows a quadrupolar signal related to prismatic Na which indicates that a pure P2 structure is obtained as previously reported,[26] see Figure S1 in the Supporting Information. **Figure 1**a presents the $^{6/7}Li$ spectra that were recorded for MNL to study the location of the lithium ions. The ^7Li isotope is more abundant and has a higher gyromagnetic ratio and quadrupolar character compared to ^6Li, and therefore typically gives rise to many magic-angle spinning sidebands (marked with asterisks) leading to strong signal overlap, which complicates analysis. The ^6Li spectrum, however, shows much weaker signal intensity due to its much smaller polarization. From the ^6Li spectrum, it can be observed that there are two signals centered at 1750 and 750 ppm. Previous studies[11,27] suggest that the signal at 1750 ppm originates from Li^+ in the TMO layer and the signal at 750 ppm originates from Li^+ in the Na layer. Quantitative analysis shows that around 46% of the lithium ions are located in the Na layer while around 54% are located in the TMO layer. It is of note that this differs from our previous study on the compound $Na_{0.8}Mn_{0.6}Fe_{0.2}Li_{0.2}O_2$ for which most of the Li^+ was found to reside in the TMO layer.[28] This might be due to the different Na contents (0.67 Na^+ per formula unit compared to 0.8), suggesting that decreasing the Na content leads to increased occupancy of the Na layer by Li^+. At the moment, these multi-element compounds are too complex to make more explicit statements on the ion occupancy. The side bands are not preferred for quantitative analysis, whereas they are good indicators of the coordination environment, e.g. limited and periodical signals of side bands apparently reflect an ordering coordination.[29] In our case, the complex composition of the material leads to the development of many side bands with varying peak intensity and position, indicating that the presence of Li^+ disorders the octahedral ion distribution.

XRD patterns of the as-synthesized materials are shown in Figure 1b and Figure S2 (Supporting Information). MNL and

Prof. T. Rojo
Inorganic Chemistry Department
University of the Basque Country
Bilbao 48080, Spain

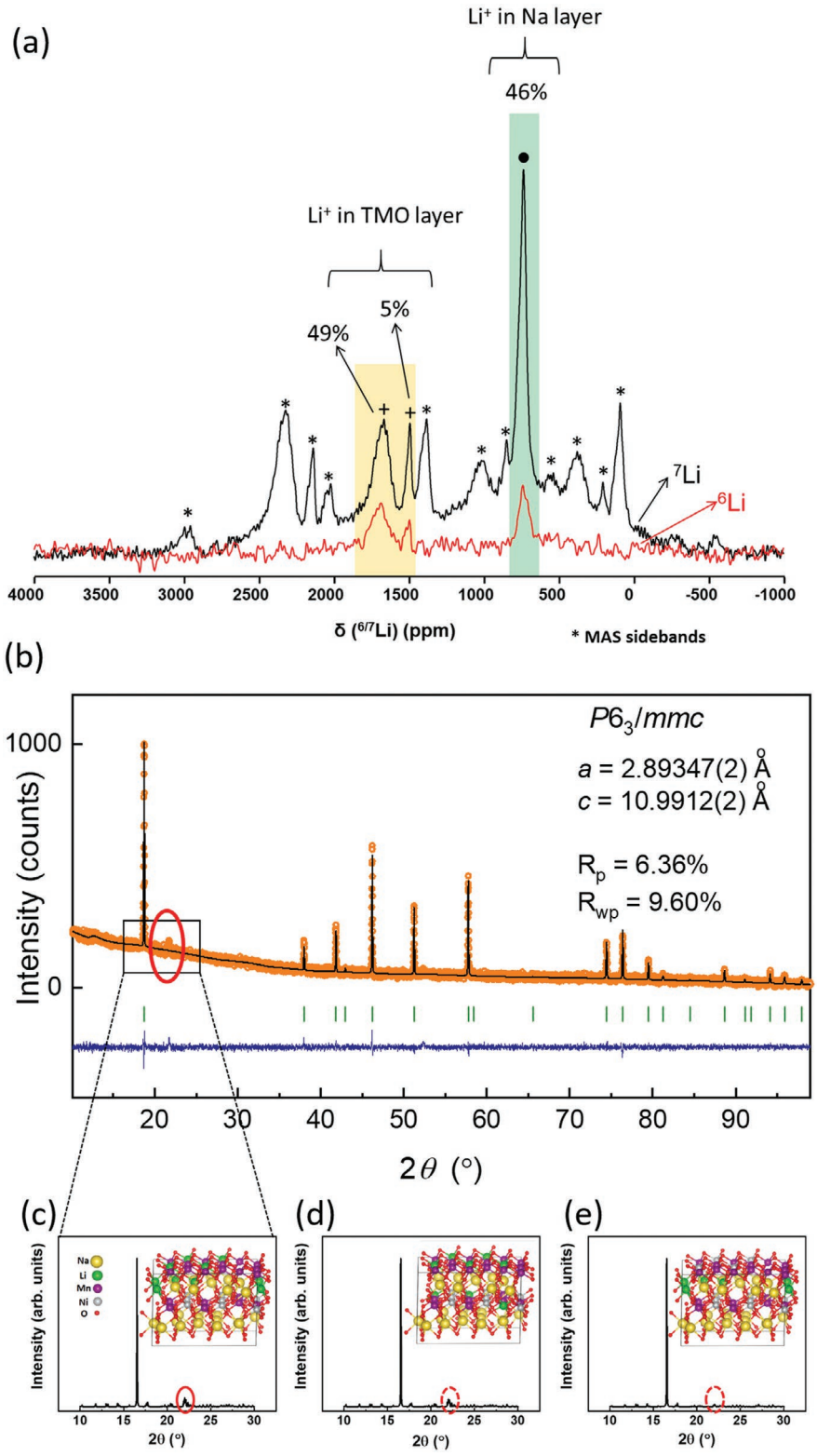

Figure 1. Structural properties of the as-synthesized material of MNL: a) ssNMR spectra of ^{6}Li (red line) and ^{7}Li (black line). Asterisks mark the MAS rotational sidebands. The plus signs mark the chemical shift of Li in the TMO layers, and the dot marks the chemical shift of Li in Na layers. b) Experimental XRD pattern (Co-radiation, $\lambda = 1.7889$ Å) of MNL together with the calculated pattern (black solid line) based on Rietveld analysis, and a residual curve (blue), with lattice parameters and *R*-factors. The green marks show the Bragg positions of the P2 phase. Simulated XRD patterns for MNL with distribution of c) equal number of Li^+ in Na and TMO layers, d) all Li^+ in TMO layers, and e) all Li^+ in one Na layer.[31]

MN41 adopt a P2 structure with $P6_3/mmc$ symmetry, while the MN32 sample shows a majority phase of P2 along with some impurities due to the increased Ni content. The small reflection observed at around 22.2° 2θ in sample MN41 (Figure S2, Supporting Information) might be due to the development of a partial ordering of metal cations in the TM slab.[30] A similar set of reflections in the range of $20° \leq 2\theta \leq 30°$ has also been observed in Li-substituted sodium layered oxides with P-type structure, for example $Na_{5/6}Li_{5/18}Mn_{13/18}O_2$, which was attributed to a Li/Mn ordering.[25] A small reflection was also found at 21.7° 2θ in the X-ray diffraction pattern of MNL (Figure 1b), which was not convolved within the Rietveld analysis. A structural model for Rietveld refinement is presented in Table S1. It includes two separate Na-sites and randomly distributed Ni-, Mn-, and Li-atoms in the TM slab (Li_{TM}). A refined total Na-occupancy of 0.63(3) is in a good agreement with the results of chemical analysis. The occupancy numbers for Li and transition metal cations as well as oxygen anions were fixed to 100% according to the chemical formula. Additionally, a possible mixed occupancy of the Na-sites by Na- and Li-atoms (Li_{Na}) was also considered. We tested two different structure models and compared them with the experimental XRD data, one with Li-atoms randomly distributed exclusively on the Na-sites ($1Li_{Na}$), and the other with an equal distribution of Li-atoms between the Na- and TM-sites ($0.5\ Li_{Na} + 0.5\ Li_{TM}$). Nearly the same R-factors were obtained in both cases ($R_p = 6.38\%$, $R_{wp} = 9.63\%$, and $R_p = 6.37\%$, $R_{wp} = 9.61\%$, respectively). Therefore, based solely on the XRD method, we cannot unambiguously confirm a possible mixed occupancy of Na and Li atoms in MNL as a result of the weak scattering factor of Li. We further simulated XRD patterns of structures from the DFT calculations, where Li^+ was either equally distributed within the Na and TMO layers, or only distributed in individual TMO or Na layers, see Figure 1c,d,e. Notable reflections between 20° and 25° (2θ) only appear when Li^+ either equally occupied the Na and TM sites, or when all Li^+ is located on TM sites. The results clearly illustrate that some structural features can only be resolved by additional methods such as NMR (in our case) or neutron scattering.

Overall, the structural analysis by NMR and XRD reveals that all materials exhibit a P2 structure, and that the lithium is roughly equally distributed in the Na layer and the TMO layer. This distribution of Li is emphasized by adopting the formula $Na_xLi_{0.1}[Mn_{0.6}Ni_{0.2}Li_{0.1}]O_2$ during discussion. The Li in the square brackets is indicative of the Li^+ content in the TMO layer, while the Li outside the square brackets reflects that which resides in the Na layer.

2.2. Electrochemical Properties

The electrochemical properties of all materials were tested between 2.0 and 4.6 V. MN32 and MN41 (Figure S3, Supporting Information) show three plateaus that originate from the redox reaction of the TMs along with superstructure formation and a P2 → O2 phase transition.[31–33] This behavior (along with superstructure formation) is completely suppressed in the MNL sample, leading to a solid solution-type ion storage mechanism as studied further below using operando XRD. The voltage profile is clearly smoothed after lithium substitution (**Figure 2**a; Figure S4, Supporting Information), indicating that the inclusion of lithium leads to a more solid solution-type ion storage mechanism. Many voltage steps were observed in most previously published sodium layered oxides. Delmas and coworkers reported that the ordering of Na/vacancies leads to multiple plateaus during desodiation.[34] Also Ceder and coworkers suggested that the multiple voltage steps of $NaMnO_2$ are also related to Na/vacancy ordering.[35] In this case, Li^+ might reduce the ordering of Na/vacancies upon de/intercalation.[31,33] This is because Li ions change the O—A—O (A = Li or Na) interaction, see section 2.4. Figure 2b shows the rate capability of the MNL electrode between 0.1 C and 2 C. At a C-Rate of 1 C (1 C = 100 mA g^{-1}), the capacity is 78 mAh g^{-1}. No capacity loss is observed after returning to 0.1 C at the end of the test. The excellent capacity retention is also seen from Figure 2c, which shows a discharge capacity over 110 mAh g^{-1} after 100 cycles. This is different from what is generally observed in P2 phase materials which tend to show capacity fading due to P2 → O2 phase transitions.[31,34,36] This behavior (along with superstructure formation) is completely suppressed in the MNL sample, leading to a solid solution-type ion storage mechanism as discussed further below using operando XRD. Although it shows a relatively lower capacity compared to the reported analogues, its capacity retention is significantly better.[22,28,37] This implies that the Li effectively prevents the formation of the O2 structure during electrochemical cycling, thereby improving cycle life.

2.3. Structural Features upon Cycling

To investigate the lattice occupation of both alkali ions (Li^+ and Na^+) during cycling, ssNMR spectra of ^7Li and ^{23}Na were recorded for electrodes at selected charge/discharge states: pristine, after desodiation (@4.6 V), and after resodiation (1st and 10th cycle@2.0 V). When the electrodes were charged to 4.6 V (**Figure 3**a), the ^{23}Na NMR signal shifts from 1750 ppm to around 1200 ppm. This is caused by a change in the valence state of the TMs.[17,20,38] After resodiation (1st and 10th cycle), the peak has shifted back to the original position, indicating the structural stability of the compound. The corresponding ^7Li spectra (Figure 3b) show that the peaks at 1750 and 750 ppm are well maintained as well. In contrast to the previously reported P2/O3 biphasic material $Na_{0.8}Mn_{0.6}Ni_{0.2}Li_{0.2}O_2$, there is no significant change in relative peak intensities in this case.[28] This shows that the lithium ions remain in the structure during cycling, thereby maintaining the disordering of the octahedral ions.

The phase of the MNL electrode was studied using operando XRD using synchrotron radiation. Figure S5a in the Supporting Information shows the electrochemical charge and discharge profiles of the operando cell (1st cycle). The capacities obtained in the operando cell were in agreement with the coin cell experiments. Figure S5c,d shows the contour plot and enlarged (002) reflection collected by operando synchrotron diffraction. No new peaks are found, but a slight peak shift is observed. A Rietveld fit was applied to analyze the lattice parameters and the unit cell volume, see Figure 3c,d and Figure S5b (Supporting Information). The change of the lattice parameter a during charging is 0.06 Å, while 0.07 Å are gained during the subsequent discharging

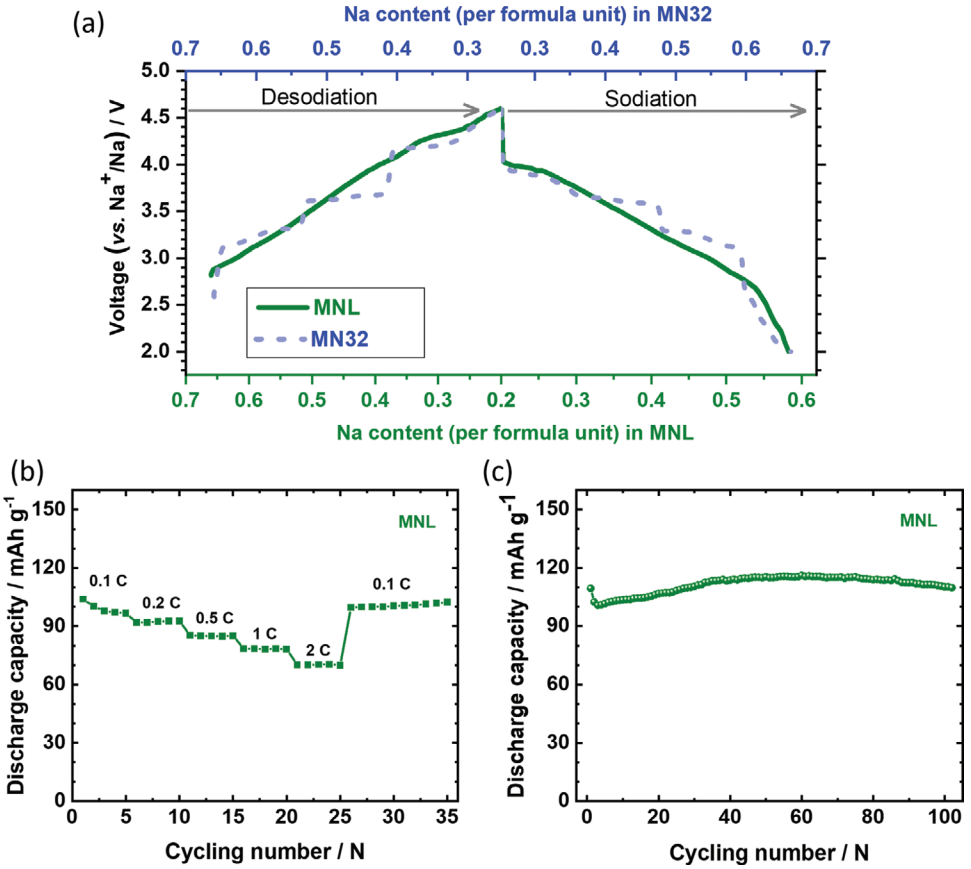

Figure 2. Electrochemical properties of MNL electrode measured in a two-electrode cell with sodium as the counter electrode: a) The voltage profiles for the first cycle of MN32 (blue) and MNL (green) electrodes. b) Rate capability of MNL at 0.1 C, 0.2 C, 0.5 C, 1 C, and 2 C. c) Capacity retention over 100 cycles of MNL at 0.1 C. (1 C = 100 mA g^{-1}).

(sodiation). Larger changes are observed for the lattice parameter *c* with a total expansion of up to 0.29 Å during charging and a reduction of up to 0.31 Å after discharging. Note that the *c* parameter shows an expansion maximum at $x = 0.2$. The contraction of the lattice parameter *a* during desodiation is caused by two effects. Firstly, the decrease in Na concentration weakens the repulsive interaction between Na^+ ions in the Na layer. Secondly, and more importantly, the oxidation of the TMs strengthens the TM-O bonds. The expansion of the lattice parameter *c* during desodiation originates from the increased O-O inter-planar electrostatic repulsion between the TMO layers.[39] Further details on this will be discussed in the next section. Overall, however, the observed changes are quite small. For comparison, one would expect much larger and more sudden changes in the case of a P2 → O2 phase transition. For example, Dahn and coworkers observed a reduction in the *c* lattice parameter by about 2.8 Å resulting from the P2 → O2 phase transition in P2-$Na_{2/3}Ni_{1/3}Mn_{2/3}O_2$ once the Na content became less than 1/3 during charging.[32] The same effect has been observed by Meng and coworkers with a change of about 2.3 Å.[40] For the MNL composition discussed herein, the observed changes in the lattice parameters *a* and *c*, alongside the negligible changes in the structure volume suggest that the phase transition (P2 → O2) is successfully suppressed during de/sodiation.

2.4. Computational Study

A further understanding of the lattice parameter changes and mechanism of charge/discharge was obtained through DFT (Density Functional Theory) calculations on compositions of $Na_xLi_{0.1}[Mn_{0.6}Ni_{0.2}Li_{0.1}]O_2$. Variation of lattice parameters and interlayer distances (**Figure 4**a,a') as well as atomic structures (Figure 4b,b'; Figure S6, Supporting Information), spin density differences (SDD, Figure 4c,c'), and number of unpaired electrons on various ions (N_{unp}, Figure S7, Supporting Information) upon sodiation/desodiation (represented by Na concentration *x*) were simulated using both DFT-PBE (Perdew–Burke–Ernzerhof) and DFT-PBE+*U* (*U*: Hubbard correction parameter) methods. We concentrated on varying Na concentrations within this structure in an effort to simulate the processes occurring during charge and discharge, with a focus on $Na_{0.67}Li_{0.1}[Mn_{0.6}Ni_{0.2}Li_{0.1}]O_2$ (MNL) and $Na_{0.33}Li_{0.1}[Mn_{0.6}Ni_{0.2}Li_{0.1}]O_2$ which experimentally demonstrated the lowest and highest *c* values, respectively, as well as $Na_{0.17}Li_{0.1}[Mn_{0.6}Ni_{0.2}Li_{0.1}]O_2$ which was the endpoint of charging during our experiments.

Both PBE and PBE+*U* calculate *a* in fair agreement with our experimental data. However, PBE performs better than PBE +*U* for computing $c(x = 0.33)$–$c(x = 0.17)$. The underestimation of $c(x = 0.17)$ with the PBE+*U* method is not directly related to the

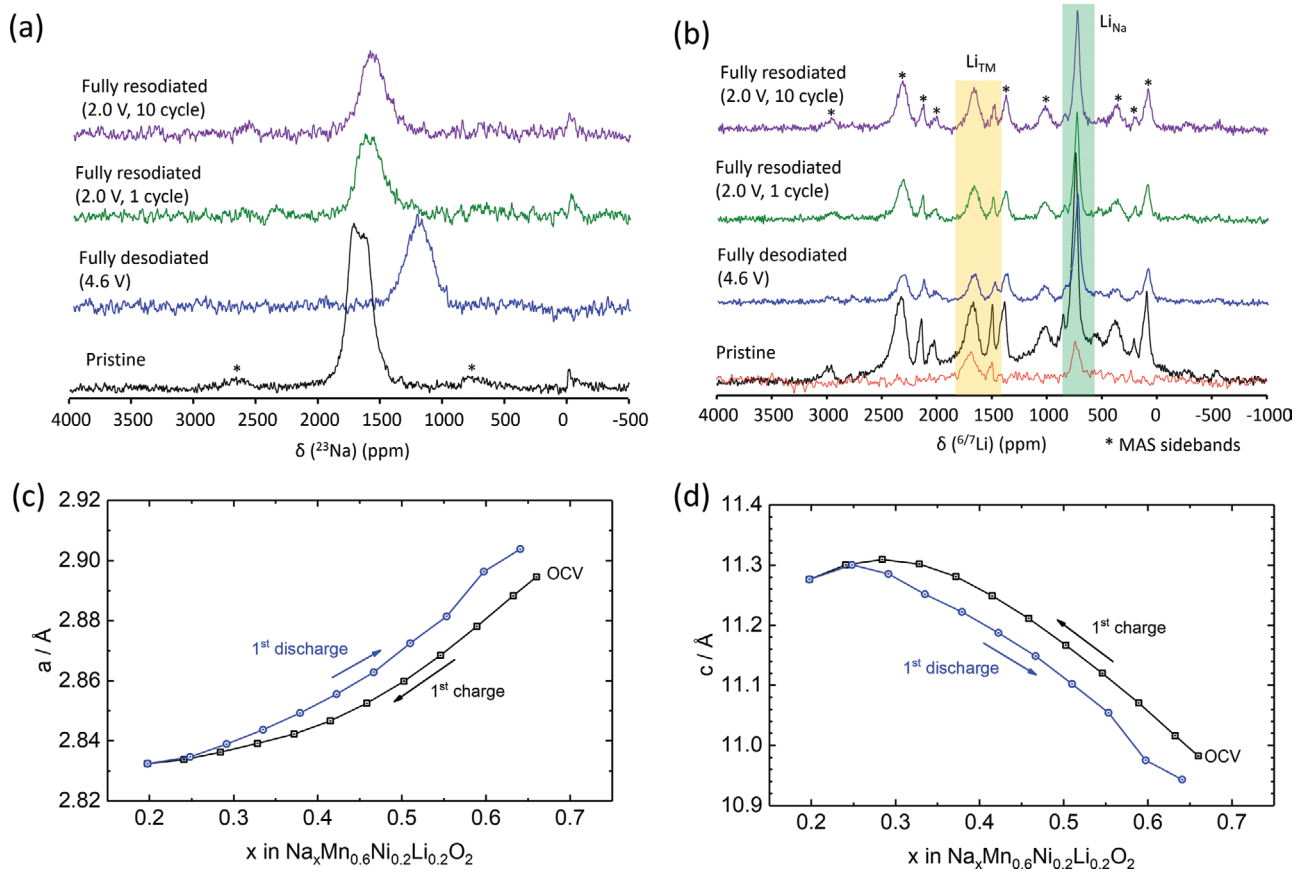

Figure 3. Structure properties of MNL during cycling: ssNMR spectra of a) ^{23}Na and b) $^{6/7}$Li at different states of charge including fully desodiated (4.6 V), and fully resodiated (1st and 10th cycles, 2.0 V). The red line in (b) indicates ^{6}Li signals. c) *a* and d) *c* lattice parameter changes during the initial de/sodiation.

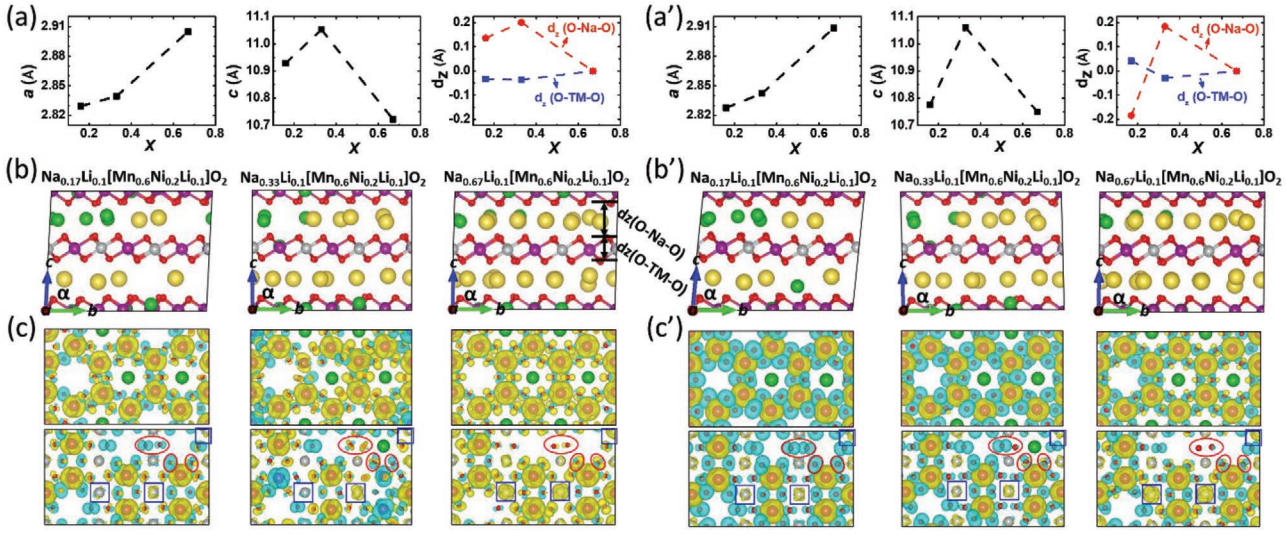

Figure 4. DFT calculations: Calculated lattice parameters and average interlayer and intralayer O—O separations of $Na_xLi_{0.1}[Mn_{0.6}Ni_{0.2}Li_{0.1}]O_2$ ($x = 0.17$, 0.33, and 0.67) as function of Na concentration *x* using a) PBE and a') PBE+*U* as well as computed atomic structures (Na: yellow, Li: green, Mn: purple, Ni: grey, O: red) of $Na_xLi_{0.1}[Mn_{0.6}Ni_{0.2}Li_{0.1}]O_2$ with b) PBE and b') PBE+*U* and corresponding spin density differences (an isosurface of 0.006 eV Å^{-3}) with c) PBE and c') PBE+*U* The up- and down-spin electrons are in yellow and blue, respectively.

Hubbard correction, but to the geometry optimization. Optimization of the PBE structure with PBE+U leads to the migration of more Li ions from TM to Na sites. This will be discussed further.

DFT calculations have been shown to be a powerful tool to quantitatively predict the proportion of elemental oxidation states.[41] As expected, both PBE and PBE+U with U(Ni) = 3.0 eV and U(Mn) = 3.0 eV predict (Figure S7, Supporting Information) that in $Na_{0.67}Li_{0.1}[Mn_{0.6}Ni_{0.2}Li_{0.1}]O_2$ 5/8 Ni^{4+} and 3/8 Ni^{3+} co-exist and the charge states of all Mn cations (Figure S7, Supporting Information) are about 4+. These results demonstrate that 5/8 of Ni as well as all Mn have their normal maximum charge states in the sodiated state. Very small SDD features with yellow colors, i.e., up-spin electrons, (Figure 4c,c′) on 5/8 Ni cations confirm their charge states to be 4+. With the desodiation from x = 0.67 to x = 0.33, both PBE and PBE+U indicate that all Ni^{3+} cations are oxidized to Ni^{4+}, i.e., SDD features on these Ni cations (highlighted by blue squares in Figure 4c,c′) become smaller. Computed N_{unp} values in Figure S7 in the Supporting Information also clearly indicate that all Ni cations are oxidized to around 4+ for 0.33 ≥ x. However, PBE+U predicts a different redox mechanism on Mn and O than PBE for 0.33 ≥ x. Although the later method shows that mainly the Mn^{4+} cations are further oxidized, the former indicates that mainly O^{2-} is oxidized. For example, with DFT-PBE we find that for the $Na_{0.33}Li_{0.1}[Mn_{0.6}Ni_{0.2}Li_{0.1}]O_2$ structure, 10/20 and 2/20 Mn have charge states of about +5 and +6, respectively (Figure S7, Supporting Information). The 2/20 Mn^{6+} cations are accompanied by 2/20 Mn^{3+} to reduce the electrostatic repulsion between their possible initial charges, namely Mn^{5+} and Mn^{4+}. Wolverton also predicted the $Mn^{4+/5+}$ redox in the Mn-based oxide for batteries by a DFT study.[42] Cabana et al. also observed Mn^{5+} in the fully charged Mn-based cathode material.[43] Oxidation of a few O^{2-} can also be observed in our computed N_{unp} plot (Figure S7, Supporting Information) for PBE. DFT-PBE+U, however, predicts that a large number of O anions undergo significant oxidation when 0.33 ≥ x, which can be clearly recognized in Figure S7 (Supporting Information) and Figure 4c′ (for example see the left O inside the red circle). A slight oxidation of several Mn cations is also observed from the PBE+U calculation in Figure S7 in the Supporting Information. At the highly charged state, PBE predicts 16/20 Mn cations have charge states of about +5 in $Na_{0.17}Li_{0.1}[Mn_{0.6}Ni_{0.2}Li_{0.1}]O_2$ (see Figure S7 in the Supporting Information) and some O anions undergo oxidation as well. However, PBE+U shows that the majority of O anions are clearly oxidized from x = 0.33 to x = 0.17 (for example see the right O inside the red circle in Figure 4c′). It should be considered that i) both PBE+U and PBE give similar results on lattice parameters and atomic structures, but ii) the former method is expected to compute the electronic structure of 3d TMs more accurately. Thus, it is observed that both O and Mn undergo oxidation during charging, but the O is probably the more active ion. As mentioned, Wolverton also predicted the coexistence of $Mn^{4+/5+}$ and anion redox in a Mn-based positive material.[42] The confirmation of the $Mn^{4+/5+}$ redox couple is the subject of further experiments that are beyond the scope of this manuscript. It should be mentioned, however, that even in the much more studied lithium layered oxides, that the discussion on oxygen redox in Mn-rich layered compounds is quite controversial and still not conclusive. For example, van der Ven and coworkers favor Mn redox over O redox based on theoretical studies.[44] On the other hand, it is also important to stress that a complete theoretical treatment of layered oxides with vacancies and mixed occupations on several sites accompanied by the partial oxidation of oxygen anions is challenging due to their complexity. Impurities due to CO_2 (formation of carbonates during calcination) and water (e.g., OH^- instead of O^{2-} at the surface, protons) can also alter the materials properties as well but we do not believe that the surface effects can impact the main conclusions from our calculations.[36,45]

To study the non-monotonic variation of c with Na concentration x, we evaluated the interlayer and intralayer O–TM–O separations (Figure 4a,a′), namely d_z(O—Na—O) and d_z(O—TM—O), respectively. It is clearly seen that from x = 0.67 to x = 0.33 the expansion of d_z(O—Na—O) is larger than the contraction of d_z(O—TM—O) leading to the expansion of c. Since this result is found with both PBE and PBE+U calculations, the desodiation-induced expansion of d_z(O—Na—O) is proposed to be due to (i) a weakening of the total attractive electrostatic O—Na—O interaction because of the removal of Na, and more importantly (ii) migration of one Li ion (out of 8 per unit cell) from the Na to TM layer. The Li ion migration from its initial position in the Na layer into a free TM site takes place through geometric optimization. This migration can occur because there are 0.1 (per formula unit) vacancies in the TMO layer in the initial state, as determined by the ssNMR measurements. This results in a weaker attractive O—Na/Li—O interaction. The contraction of d_z(O—TM—O) is mainly caused by the reduction of the radii of the Ni cations and strengthening of O—TM—O bonds with the oxidation of Ni. Oxidation of Mn (predicted by PBE) and O (predicted by PBE+U) are not the dominant factors in controlling the lattice parameter change, as both functionals give similar results from x = 0.67 to x = 0.33. For desodiation from x = 0.33 to x = 0.17, the contraction of d_z(O—Na—O) can be attributed to primarily originating from the following two causes. i) The O—TM—O layers start to slide with respect to each other and pack as closely as possible to optimize the overall electrostatic interactions. This can be seen in Figure 4b′ where the α angle slightly decreases from 88.99° (x = 0.67) to 84.62° (x = 0.17) with the PBE+U approximation. ii) more Li ions occupy the Na layers leading to a stronger O—Na/Li—O attraction. PBE calculation predicts two Li ions to migrate from TM to Na (5/8 Li ions in Na layers), but PBE+U predicts migration of three Li ions (6/8 Li ions in Na layers). This is most likely driven by electrostatic forces. Migration of Li ions from the TMO to Na layer, where a large number of vacant sites exist, reduces the TM-Li repulsion. Since the magnitude of the change in d_z(O—TM—O) is not as large as that of d_z(O—Na—O) during desodiation from x = 0.33 to x = 0.17, the c value decreases (based on PBE and PBE+U) as a result of the two aforementioned reasons. It is predicted that the increase in d_z(O—TM—O) with the PBE +U functional is probably due to the weakening of attraction between TMs, whose charge states do not change significantly, and the oxidation of O.

The migration of Li from Na to TMO layers or vice versa is in fact the most important parameter to determine the c value. For this reason, the decrease in c is larger in the PBE+U calculations (3/8 → 6/8 Li ions in Na layers) than that with PBE (3/8 → 5/8 Li ions in Na layers) for x = 0.33 → x = 0.17. This is also true for $Na_{0.67}Li_{0.1}[Mn_{0.6}Ni_{0.2}Li_{0.1}]O_2$ where the value of c in a studied

structure with 6/8 Li ions is 0.06 Å shorter than that with 4/8 Li ions in Na layers. This can explain the reason behind the contraction of the *c* value after the first discharge (Figure 3d). Moreover, we find that the distribution of Li ions in the Na layers does not influence the *c* value as much since a $Na_{0.67}Li_{0.1}[Mn_{0.6}Ni_{0.2}Li_{0.1}]O_2$ structure with 2 Li ions at each Na layer (concentration of Li ions in Na layers = 4/8) has a similar *c* value to that presented in Figure 4a with 4/8 Li ions at every second Na layer. However, it is difficult to quantify the Li^+ distribution for the intermediate charged electrode (i.e., $Na_{0.33}Li_{0.1}(Mn_{0.6}Ni_{0.2}Li_{0.1})O_2$) by ssNMR due to its relatively poor stability.

Overall, our DFT-PBE calculations show that the P2 phase is more favorable than the O2 counterpart by 164 meV (per primitive unit cell) and 16 meV (per primitive unit cell) in the cases of $Na_{0.67}Li_{0.1}[Mn_{0.6}Ni_{0.2}Li_{0.1}]O_2$ and $Na_{0.17}Li_{0.1}[Mn_{0.6}Ni_{0.2}Li_{0.1}]O_2$, respectively. This result confirms that the stability of the P2 phase is preserved during charging.

3. Conclusion

Our study unravels the role of lithium defects for improving the cycle life of Ni/Mn-based layered oxides as cathode materials for SIBs. The lithium-substituted (MNL, $Na_{0.67}Mn_{0.6}Ni_{0.2}Li_{0.2}O_2$) and unsubstituted (MN32 and MN41, $Na_{0.67}Mn_{0.6}Ni_{0.4}O_2$ and $Na_{0.67}Mn_{0.8}Ni_{0.2}O_2$, respectively) materials were prepared by a sol-gel synthesis followed by a high temperature calcination. All as-synthesized materials showed a P2 structure, but demonstrated clear differences in their voltage profiles. While the voltage profile for MN32 and MN41 showed several steps due to ordering phenomena and phase transitions, introducing lithium leads to a solid-solution type behavior in MNL and also a much better cycle life. To understand the underlying reasons for the behavior of MNL, (operando) XRD, ssNMR and DFT calculations were applied. ssNMR revealed that the lithium ions are almost equally distributed in the Na layer (46%) and TMO layer (54%). The same ratio was found after cycling. Results from operando XRD showed that the changes in lattice parameters are small, indicating stability of the P2 structure during cycling. However, the *c* lattice parameter first increases and then decreases. DFT calculations showed that this behavior is due to the dynamic redistribution of lithium ions during cycling. Li ions first migrate to TM sites leading to a lattice expansion in the *c*-direction ($x = 0.67$ to $x = 0.33$). Below $x < 0.33$, Li ions migrate back to the Na sites leading to a shrinkage in the *c*-direction. The reversible capacity of MNL was around 110 mAh g^{-1} with negligible capacity loss over 100 cycles. DFT calculations suggest that the capacity arises from Ni^{3+}/Ni^{4+} and $O^{2-}/O^{2-\delta}$ redox processes, although Mn^{4+}/Mn^{5+} also contributes to a small degree. Overall, this study clarifies how lithium defects improve the Na storage in $Na_{0.67}Mn_{0.6}Ni_{0.2}Li_{0.2}O_2$. Lithium stabilizes the P2 phase and redistributes between the Na and TMO layers during charging/discharging.

Supporting Information

Supporting Information is available from the Wiley Online Library or from the author.

Acknowledgements

P.A. and T.R. thank for support within for LIBRA project within the EIG Concert Japan program financed by BMBF (01DR18003), MINECO, and JST. L.Y. thanks the China Scholarship Council for funding and the support within SIAT Innovation Program for Excellent Young Researchers (No. E1G028). P.K. gratefully acknowledges the financial support from "Bundesministerium für Bildung und Forschung" (BMBF) as well as the computing time granted through JARA-HPC on the supercomputer JURECA at Forschungszentrum Jülich. The authors acknowledge Dr. A. Missyul (ALBA synchrotron, Barcelona, Spain) for the help during operando XRD experiments. The operando XRD experiments were performed at BL04-MSPD beamline at ALBA Synchrotron.

Open access funding enabled and organized by Projekt DEAL.

Conflict of Interest

The authors declare no conflict of interest.

Author Contributions

L.Y. and P.A. conceived the idea for the work. L.Y. and P.K.N. synthesized the materials, performed XRD of MN32&41 and all electrochemical properties. S.M., D.M., and L.G. performed the (operando) XRD and carried out the refinement. NMR studies were done by J.M.L.d.A. and L.Y. The DFT calculation and XRD simulations were carried out by P.K. and L.-Y.K. The manuscript was written by L.Y. and P.A. and was edited by all authors. All authors contributed to the discussions.

Data Availability Statement

The data that support the findings of this study are available from the corresponding author upon reasonable request.

Keywords

DFT, layered oxides, Li doping, $Na_{0.67}Mn_{0.6}Ni_{0.2}Li_{0.2}O_2$ cathodes, sodium ion batteries, ssNMR, XRD

Received: April 27, 2021
Revised: June 16, 2021
Published online: July 6, 2021

[1] a) P. Adelhelm, *Angew. Chem., Int. Ed.* **2018**, *57*, 6710; b) Y.-S. Hu, S. Komaba, M. Forsyth, C. Johnson, T. Rojo, *Small Methods* **2019**, *3*, 1900184.
[2] N. Yabuuchi, K. Kubota, M. Dahbi, S. Komaba, *Chem. Rev.* **2014**, *114*, 11636.
[3] M. H. Han, E. Gonzalo, G. Singh, T. Rojo, *Energy Environ. Sci.* **2015**, *8*, 81.
[4] a) C. Vaalma, D. Buchholz, M. Weil, S. Passerini, *Nat. Mater.* **2018**, *3*, 18013; b) Y. E. Durmus, H. Zhang, F. Baakes, G. Desmaizieres, H. Hayun, L. Yang, M. Kolek, V. Küpers, J. Janek, D. Mandler, S. Passerini, Y. Ein-Eli, *Adv. Energy Mater.* **2020**, *10*, 2000089.
[5] P. K. Nayak, L. Yang, K. Pollok, F. Langenhorst, L. Wondraczek, P. Adelhelm, *Batteries Supercaps* **2018**, *2*, 104.
[6] P. K. Nayak, L. Yang, W. Brehm, P. Adelhelm, *Angew. Chem., Int. Ed.* **2018**, *57*, 102.

[7] a) K. Kubota, S. Kumakura, Y. Yoda, K. Kuroki, S. Komaba, *Adv. Energy Mater.* **2018**, *8*, 1703415; b) N. Sabi, A. Sarapulova, S. Indris, S. Dsoke, V. Trouillet, L. Mereacre, H. Ehrenberg, I. Saadoune, *J. Power Sources* **2021**, *481*, 229120.
[8] N. Ortiz-Vitoriano, N. E. Drewett, E. Gonzalo, T. Rojo, *Energy Environ. Sci.* **2017**, *10*, 1051.
[9] a) T. Wang, D. Su, D. Shanmukaraj, T. Rojo, M. Armand, G. Wang, *Electrochem. Energy Rev.* **2018**, *1*, 200; b) C. Delmas, C. Fouassier, P. Hagenmuller, *Physica B+C* **1980**, *99B*, 81; c) C. Delmas, J.-J. Braconnier, C. Fouassier, P. Hagenmuller, *Solid State Ionics* **1981**, *4*, 165.
[10] C. Delmas, D. Carlier, M. Guignard, *Adv. Energy Mater.* **2020**, *11*, 2001201.
[11] R. J. Clément, P. G. Bruce, C. P. Grey, *J. Electrochem. Soc.* **2015**, *162*, A2589.
[12] A. Bhandari, J. Bhattacharya, *J. Electrochem. Soc.* **2016**, *164*, A106.
[13] E. de la Llave, E. Talaie, E. Levi, P. K. Nayak, M. Dixit, P. T. Rao, P. Hartmann, F. Chesneau, D. T. Major, M. Greenstein, D. Aurbach, L. F. Nazar, *Chem. Mater.* **2016**, *28*, 9064.
[14] E. Gonzalo, N. Ortiz-Vitoriano, N. E. Drewett, B. Acebedo, J. M. López del Amo, F. J. Bonilla, T. Rojo, *J. Power Sources* **2018**, *401*, 117.
[15] C. Fouassier, G. Matejka, J.-M. Reau, P. Hagenmuller, *J. Solid State Chem.* **1973**, *6*, 532.
[16] a) G. Singh, J. M. López del Amo, M. Galceran, S. Pérez-Villar, T. Rojo, *J. Mater. Chem. A* **2015**, *3*, 6954; b) M. H. Han, N. Sharma, E. Gonzalo, J. C. Pramudita, H. E. A. Brand, J. M. López del Amo, T. Rojo, *J. Mater. Chem. A* **2016**, *4*, 18963.
[17] R. J. Clément, J. Billaud, A. R. Armstrong, G. Singh, T. Rojo, P. G. Bruce, C. P. Grey, *Energy Environ. Sci.* **2016**, *9*, 3240.
[18] S. Kumakura, Y. Tahara, K. Kubota, K. Chihara, S. Komaba, *Angew. Chem., Int. Ed.* **2016**, *55*, 12760.
[19] D. Kim, S.-H. Kang, M. Slater, S. Rood, J. T. Vaughey, N. Karan, M. Balasubramanian, C. S. Johnson, *Adv. Energy Mater.* **2011**, *1*, 333.
[20] J. Xu, D. H. Lee, R. J. Clément, X. Yu, M. Leskes, A. J. Pell, G. Pintacuda, X.-Q. Yang, C. P. Grey, Y. S. Meng, *Chem. Mater.* **2014**, *26*, 1260.
[21] J. Xu, H. Liu, Y. S. Meng, *Electrochem. Commun.* **2015**, *60*, 13.
[22] a) X. Rong, E. Hu, Y. Lu, F. Meng, C. Zhao, X. Wang, Q. Zhang, X. Yu, L. Gu, Y.-S. Hu, H. Li, X. Huang, X.-Q. Yang, C. Delmas, L. Chen, *Joule* **2019**, *3*, 503; b) X. Rong, J. Liu, E. Hu, Y. Liu, Y. Wang, J. Wu, X. Yu, K. Page, Y.-S. Hu, W. Yang, H. Li, X.-Q. Yang, L. Chen, X. Huang, *Joule* **2018**, *2*, 125.
[23] B. Gludovatz, A. Hohenwarter, K. V. S. Thurston, H. Bei, Z. Wu, E. P. George, R. O. Ritchie, *Nat. Commun.* **2016**, *7*, 10602.
[24] H. Liu, J. Xu, C. Ma, Y. S. Meng, *Chem. Commun.* **2015**, *51*, 4693.
[25] C. Zhao, Q. Wang, Z. Yao, J. Wang, B. Sánchez-Lengeling, F. Ding, X. Qi, Y. Lu, X. Bai, B. Li, H. Li, A. Aspuru-Guzik, X. Huang, C. Delmas, M. Wagemaker, L. Chen, Y.-S. Hu, *Science* **2020**, *370*, 708.
[26] E. Gonzalo, M. H. Han, J. M. López del Amo, B. Acebedo, M. Casas-Cabanas, T. Rojo, *J. Mater. Chem. A* **2014**, *2*, 18523.
[27] M. Bianchini, E. Gonzalo, N. E. Drewett, N. Ortiz-Vitoriano, J. M. López del Amo, F. J. Bonilla, B. Acebedo, T. Rojo, *J. Mater. Chem. A* **2018**, *6*, 3552.
[28] L. Yang, J. M. López del Amo, Z. Shadike, S.-M. Bak, F. Bonilla, M. Galceran, P. K. Nayak, J. R. Buchheim, X.-Q. Yang, T. Rojo, P. Adelhelm, *Adv. Funct. Mater.* **2020**, *30*, 2003364.
[29] a) U. Maitra, R. A. House, J. W. Somerville, N. Tapia-Ruiz, J. G. Lozano, N. Guerrini, R. Hao, K. Luo, L. Jin, M. A. Perez-Osorio, F. Massel, D. M. Pickup, S. Ramos, X. Lu, D. E. McNally, A. V. Chadwick, F. Giustino, T. Schmitt, L. C. Duda, M. R. Roberts, P. G. Bruce, *Nat. Chem.* **2018**, *10*, 288; b) R. House, U. Maitra, M. Perez-Osario, J. Lozano, L. Jin, J. Somerville, M. Roberts, P. Bruce, L. Duda, A. Nag, A. Walters, K. Zhou, *Nature* **2019**, *577*, 502.
[30] K. A. Jarvis, Z. Deng, L. F. Allard, A. Manthiram, P. J. Ferreira, *Chem. Mater.* **2011**, *23*, 3614.
[31] J. W. Somerville, A. Sobkowiak, N. Tapia-Ruiz, J. Billaud, J. G. Lozano, R. A. House, L. C. Gallington, T. Ericsson, L. Häggström, M. R. Roberts, U. Maitra, P. G. Bruce, *Energy Environ. Sci.* **2019**, *12*, 2223.
[32] Z. Lu, J. R. Dahn, *J. Electrochem. Soc.* **2001**, *148*, A1225.
[33] P.-F. Wang, H.-R. Yao, X.-Y. Liu, Y.-X. Yin, J.-N. Zhang, Y. Wen, X. Yu, L. Gu, Y.-G. Guo, *Sci. Adv.* **2018**, *4*, eaar6018.
[34] R. Berthelot, D. Carlier, C. Delmas, *Nat. Mater.* **2011**, *10*, 74.
[35] X. Ma, H. Chen, G. Ceder, *J. Electrochem. Soc.* **2011**, *158*, A1307.
[36] M. H. Han, E. Gonzalo, N. Sharma, J. M. López del Amo, M. Armand, M. Avdeev, J. J. Saiz Garitaonandia, T. Rojo, *Chem. Mater.* **2016**, *28*, 106.
[37] Y. Liu, Q. Shen, X. Zhao, J. Zhang, X. Liu, T. Wang, N. Zhang, L. Jiao, J. Chen, L.-Z. Fan, *Adv. Funct. Mater.* **2020**, *30*, 1907837.
[38] R. J. Clément, J. Xu, D. S. Middlemiss, J. Alvarado, C. Ma, Y. S. Meng, C. P. Grey, *J. Mater. Chem. A* **2017**, *5*, 4129.
[39] N. Tapia-Ruiz, W. M. Dose, N. Sharma, H. Chen, J. Heath, J. W. Somerville, U. Maitra, M. S. Islam, P. G. Bruce, *Energy Environ. Sci.* **2018**, *11*, 1470.
[40] D. H. Lee, J. Xu, Y. S. Meng, *Phys. Chem. Chem. Phys.* **2013**, *15*, 3304.
[41] a) L.-Y. Kuo, O. Guillon, P. Kaghazchi, *J. Mater. Chem. A* **2020**, *8*, 13832; b) N. Voronina, H. J. Kim, A. Konarov, N. Yaqoob, K.-S. Lee, P. Kaghazchi, O. Guillon, S.-T. Myung, *Adv. Energy Mater.* **2021**, *11*, 2003399.
[42] C. Wolverton, *2018 Meet. Abstr.* **2018**, *185*, MA2018.
[43] J. Cabana, G. Rousse, A. Fuertes, M. R. Palacín, *J. Mater. Chem.* **2003**, *13*, 2402.
[44] a) E. Goikolea, V. Palomares, S. Wang, I. R. Larramendi, X. Guo, G. Wang, T. Rojo, *Adv. Energy Mater.* **2020**, *10*, 2002055; b) M. D. Radin, J. Vinckeviciute, R. Seshadri, A. Van der Ven, *Nat. Energy* **2019**, *4*, 639; c) E. Gonzalo, M. Zarrabeitia, N. E. Drewett, J. M. López del Amo, T. Rojo, *Energy Storage Mater.* **2021**, *34*, 682.
[45] P.-F. Wang, Y. You, Y.-X. Yin, Y.-G. Guo, *Adv. Energy Mater.* **2018**, *8*, 1701912.